Springer

KSME

Journal of Mechanical Science and Technology 33 (2) (2019) 903~912
www.springerlink.com/content/1738-494x(Print)/1976-3824(Online)
DOI 10.1007/s12206-019-0147-y

Computational investigation on secondary flows in a linear turbine cascade with tapered dual fence †

Kiran K. N., Sushanlal Babu and Anish S.*

Turbomachinery Laboratory, Department of Mechanical Engineering, National Institute of Technology Karnataka, Mangalore-575025, India

(Manuscript Received April 11, 2018; Revised July 30, 2018; Accepted September 6, 2018)

Abstract

The focus of the present work is to minimize the secondary flow losses inside a linear turbine cascade by means of a novel design of streamwise dual fence. The leading edge and trailing edge of the fences have been modified so as to reduce the total pressure loss coefficient in the passage. The study has been carried out computationally based on *RANS* simulations with *SST* turbulence model. Numerous simulations have been undertaken with single fence and dual fence models and compared with the base case model. The dual fence model with tapered trailing edge exhibits significant loss reduction compared to the base case. A suitable fence height ratio (*FHR*) has been identified for the dual fence model. The *FHR = 2* configuration reduces the secondary flow kinetic energy by 78 % within the blade passage and it reduces the exit angle deviation significantly throughout the span. Detailed flow field analysis has been carried out to understand the physical mechanism behind the loss reduction with dual fence models. It is observed that fence-1 breaks the pressure side leg of the horse shoe vortex at the beginning of their formation itself. The radial penetration of the suction side leg of the horse shoe vortex is restrained by fence-2. These combined effects prevent the formation and mixing of two prominent loss core regions thereby avoiding the accumulation of low energy fluid near the suction side of blade.

Keywords: Dual fence; Streamwise fence; Secondary flow; Axial turbine

1. Introduction

In any gas turbine about one third of the total losses is attributed to secondary flow losses in low aspect ratio turbine blades. It is therefore very essential to understand the underlying physics and device mechanisms to limit these losses. Secondary loss is three dimensional in nature due to the vortical flow structure in the blade passage. Normally, gas turbine with high blade camber exhibits high flow separation and vortical flow structure. In the present work a novel design of streamwise fence is introduced to reduce the secondary flow losses in the turbine blade passage. Detailed computational simulations have been carried out in a linear turbine cascade with an objective to reduce the overall total pressure loss in the passage and minimize the exit angle deviation.

Secondary flow is always transverse to primary flow caused due to cross passage pressure gradient in the boundary layer in the blade passage [1, 2]. Detailed description of secondary flow origin and their complex development has been documented in the open literature by many researchers [3-7]. Accordingly, several methods have been suggested to reduce these losses. Commonly used methods are leading edge filleting [8-13], stream-wise fence [14-18], end wall contouring [19-22], end wall film injection [23, 24], blade thickening in the end wall region and blade lean [25] and sweep.

Streamwise fence effectively helps in reducing the secondary flow losses inside the turbine passage. Due to cross passage pressure gradient, fluid move from the pressure side of one blade to suction side of adjacent blade near the end wall. Fencing on the end wall is expected to prevent this movement and guide the flow to the exit so as to get proper incidence for next set of blade rows. However, great care has to be taken while designing the fence. An improper design may enhance the pressure loss coefficient in the passage rather than alleviating it. The important parameters needs to be considered while designing the fence are the fence profile, height and the location of the fence in the blade passage. Numerous studies have been carried out in order to optimize the fence height under different operating conditions [2, 14-16]. Kawai et al. [17] suggested that fences are more effective if the height is 1/3rd of the inlet boundary layer thickness. This is later modified by Kumar and Govardhan [2] suggesting that the optimum fence height varies linearly from 1/6th of boundary layer thickness at leading edge to 1/3th at trailing edge. Regarding the position, it is generally accepted that fence has to be located at half

*Corresponding author. Tel.: +91 9036317552
E-mail address: anish@nitk.edu.in
† Recommended by Associate Editor Joon Ahn

Table 1. Cascade blade details.

Blade inlet angle	47.6°
Blade exit angle	-68.0°
Stagger angle	-36.1°
Blade chord	224 mm
Axial chord	181 mm
Blade pitch, B	191 mm
Blade span, S	400 mm
Reynolds number (based on axial chord and exit velocity)	4.3×10^5
Exit Mach number	0.11

pitch distance from blade in order to reduce the secondary flow and exit angle deviation. The present study has been undertaken to achieve further loss reduction by optimising fence geometry, particularly at the leading and trailing edge.

The objective of the present computational study is to reduce the secondary flow by means of a novel dual fence with tapered trailing edge in a linear turbine cascade. The influence of tapering of the fence trailing edge on loss coefficient has been noted and an appropriate design has been generated. The effect of fence height ratio on the aerodynamic losses has been investigated in this study. A detailed flow field analysis is conducted on the best configuration to understand the influence of dual fence in improving the flow structure.

2. Methodology

The work has been carried out by formulating the technical aspects of the fencing the blade passage for controlled flow structure. Computational investigations have been carried out in Durham cascade [1], which is a low speed and large scale linear turbine cascade. The blades are designed to have an aerodynamic similarity same as real machines rather than geometrical similarity. The blade profile is shown in Fig. 1 and the geometrical specifications are detailed in Table 1.

2.1 Geometrical modelling and meshing

The geometrical model for the simulation consists of single blade passage, wherein the side walls are kept at one pitch distance. Five different models have been selected for the study; one without fence (model-1) and four cases with different type of fence geometries (model-2 to model-5). The computational domain for these models are shown in Fig. 2. Among these, model-1 serves as the base case. Model-2 is a single fence model whereas model-3, model-4 and model-5 are dual fence models. These models are differed by the size and nature of the fence profile used. The optimum profiling of the fence has been evolved progressively by systematically analysing the flow behaviour in each model. Detailed description of these models are given below.

The fence in model-2 is a simple uniform thickness fence

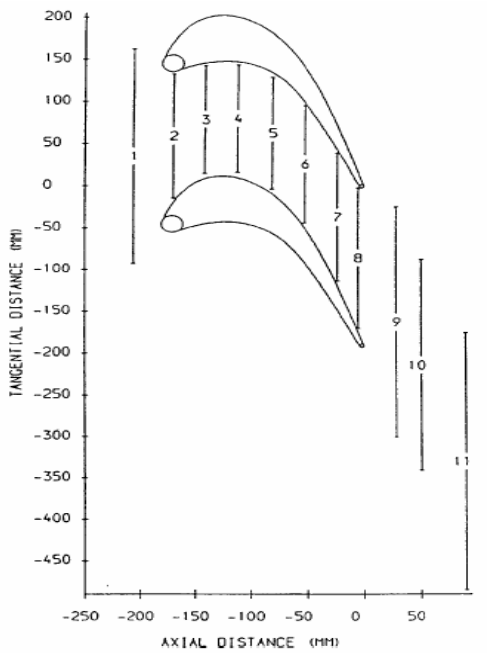

Fig. 1. Turbine blade profile and measurement location (Hartland [1]).

whose profile exactly follows the blade camber line. The last three cases are dual fence geometries. The fence which is close to pressure surface is named as fence-1 and it is kept at half pitch away from the blade camber line. The second fence (fence-2) is positioned at tangential distance of 40 mm away from the first fence. The height of second fence is 15 mm. For model-3, the fence-1 is straight from the leading edge up to an axial distance of 50 mm (X = 50 mm), thereafter it follows the blade camber till the trailing edge. On the other hand fence-2 is kept similar to the blade camber line. The chord length of the fences are shortened for improved performance for model-4. The fence-1 is not extended for full length of the blade instead it is cut from 83 % of axial chord from the leading edge of blade camber line. While fence-2 follows same curvature as that of camber line, it ends at 73 % of axial chord from the leading edge. Further improvement in the loss reduction is sought by tapering the fence near the trailing edge (model-5). The tapering is given in such a way that the height of the blade decreases linearly from a distance of 63 % of axial chord to the trailing edge of the fence. In all these models the thickness of both fences are 2.5 mm.

The geometrical modelling and meshing of the computational domain is carried out using ICEMCFD. The inlet of the fluid domain is 1.5 times the axial chord distance away from the leading edge of the blade. The outlet plane is kept at a distance of two times the axial chord distance away from the trailing edge of the blade. In order to reduce the computational effort and time only half of the span (50 % of overall span) is modelled by specifying symmetric wall condition at the mid-span region. Along the transverse direction, translational periodicity is set at one pitch length (Fig. 2(e)). The mesh around

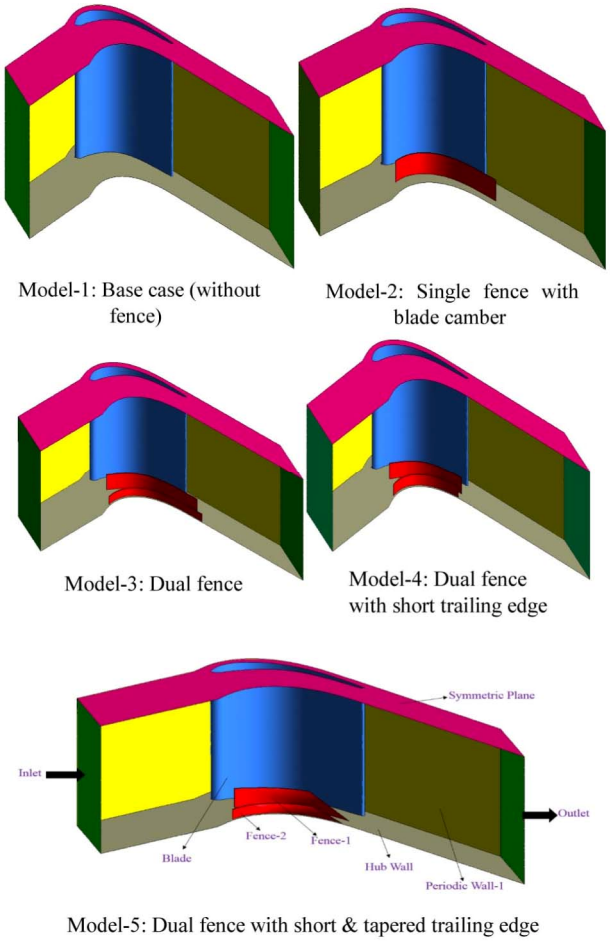

Fig. 2. Computational domains for different fence design. Model-5 shows the boundaries used in the computational domain.

the blade, hub and fence surface is fully structured and remaining flow domain is unstructured in axial and tangential direction. The maximum size of mesh size for whole domain is 3.5 mm with scale factor of 1. Fine prism layers are attached around the blade and hub surface to take care of the boundary layer effects (Fig. 3). The first cell height normal to the surface is 0.35 mm with exponential height ratio of 1.15 up to 12 layers.

2.2 Solver details

The simulations are carried out with Reynolds averaged Navier Stoke (RANS) equations and the turbulence is modelled with SST k-ω model. A commercial software ANSYS-CFX is used for the computational simulations. It solves the RANS equations in their conservation form. In the present analysis an element-based finite volume method, involving the discretization of spatial domain using tetrahedral and prism elements. All solution variables and fluid properties are stored at the nodes (mesh vertices). Volume integrals are discretized within each element sector and accumulated to the control volume to which the sector belongs. Surface integrals are discretized at the integration points located at the center of each surface segment within an element and then distributed to the adjacent control volumes. For advection terms, the high resolution scheme is used whereas for diffusion terms shape functions are used to evaluate spatial derivatives. High resolution scheme uses a second order scheme as far as possible and blends to a first order scheme to maintain boundedness. It contains far less numerical diffusion. The details of the boundary layer at the inlet region is obtained from the experimental data of Hartland et al. [1]. Accordingly, total pressure profile as shown in Fig. 4 has been specified as an inlet boundary condition. The turbulence intensity at inlet is 5 %. The selected working fluid is air, as ideal gas, which enters the domain with a static temperature of 292.15 K. At the outlet, fixed mass flow for all the domain. The domain walls are specified with no slip condition and assumed to be perfectly insulated.

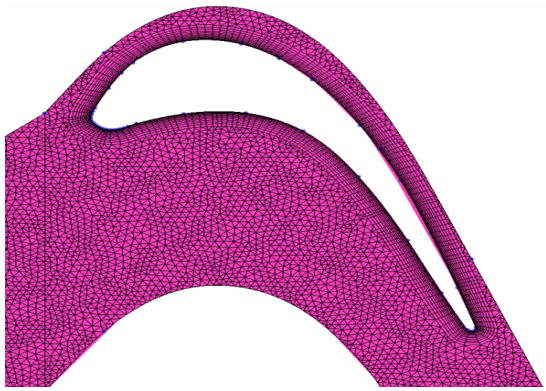

Fig. 3. The grid generated around the blade for model-1.

3. Verification and validation

The verification process examines the accuracy in the models through comparison to exact analytical results. Grid independent study is carried out with total pressure ratio as the objective function. The number of mesh elements versus total pressure ratio is shown in Fig. 5 for planar case. There is no significant change in the pressure ratio beyond 3.1 million elements hence it is chosen for further simulations. Similar studies have been undertaken for all the profiled endwall cases.

For validation purpose the yaw angle variation in the span and the pitch averaged loss coefficient variations are considered and compared with the experimental results of Hartland et al. [1]. Fig. 6 shows the spanwise variation of yaw angle calculated at 128 % of the axial chord (C_{ax}) for three different turbulence models. The shear stress transport (*SST*) model shows closer match to the experimental data than the standard k-ε and k-ω models. Hence the *SST* turbulence model has been selected for further analysis. It is noteworthy to mention that some of the previous studies also [2, 26] identified the *SST* model as the most suitable turbulence model for analyzing secondary flows.

The total pressure loss coefficient is plotted at 9 % C_{ax} dis-

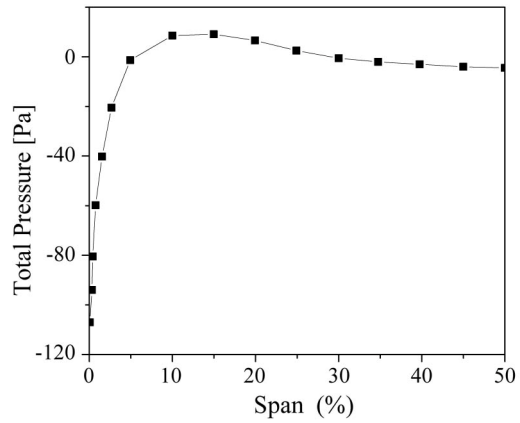

Fig. 4. Total pressure profile at inlet.

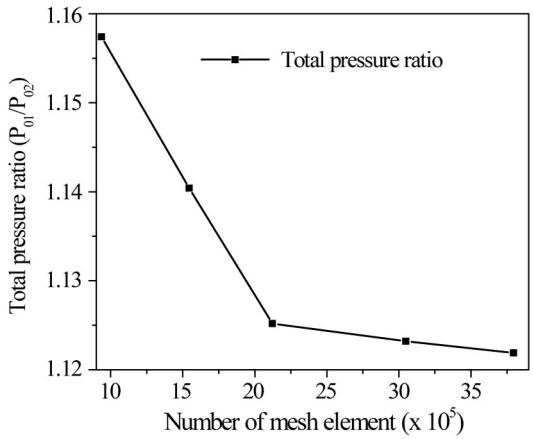

Fig. 5. Grid independence study for planar case.

tance before leading edge and at a downstream distance of 128 % C_{ax} (Figs. 7(a) and (b)). The loss coefficients are evaluated from the hub wall to midspan in the following manner.

$$\overline{C_{po}} = \frac{\int V_u \xi dT}{\int V_u dT} \tag{1}$$

$$\xi = \frac{P_{01} - P_0}{0.5\rho V^2}. \tag{2}$$

At the downstream side, the present numerical results are compared with the experimental and CFD results of Hartland et al. [1]. At the upstream location comparison is made only with the experimental data as CFD results of Hartland et al. [1] was not available for this location. Near to the endwall both CFD simulations are over predicting. From 2.5 % span to 7.5 % span present CFD simulations are predicting better than numerical results of Hartland et al. [1]. From 7.5 % span onwards the simulations are over predicting the loss coefficient values. This over prediction of loss coefficient may be attributed to several factors, the prominent being the transition nature of boundary layer near the endwall [27]. The *RANS* modelling assumes a fully turbulent boundary layer in place of a transitional boundary layer. Cui and Tucker [28] mentioned a new laminar boundary layer covers much of the endwall downstream of the pressure leg of the horseshoe vortex. Additionally, the separation from the blade surface is identified as an unsteady process with wide range of points of separation

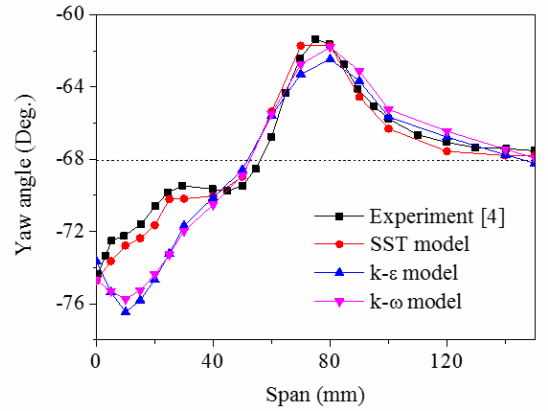

Fig. 6. Pitch averaged exit flow angle for base case at 128 %C*ax*.

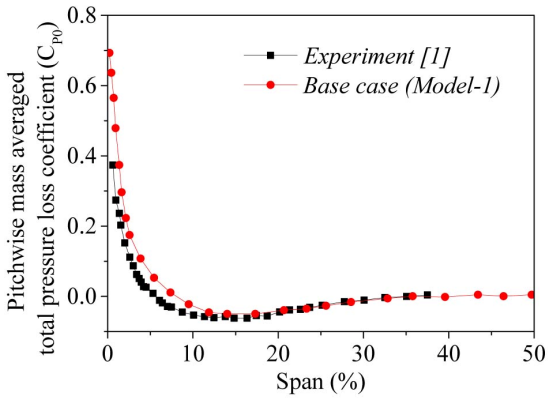

(a)

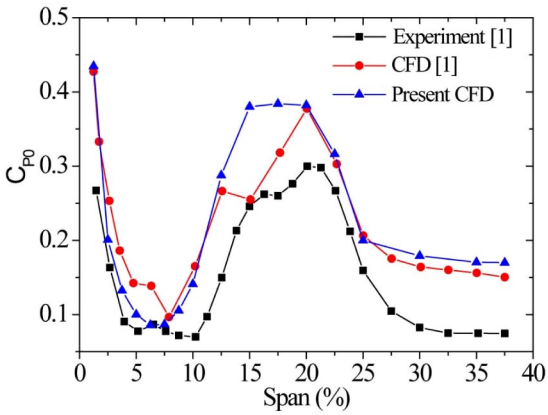

(b)

Fig. 7. Pitch averaged total pressure loss coefficient for base case (a) at 9 % C_{ax} before the leading edge; (b) at 128 % C_{ax} downstream of the trailing edge.

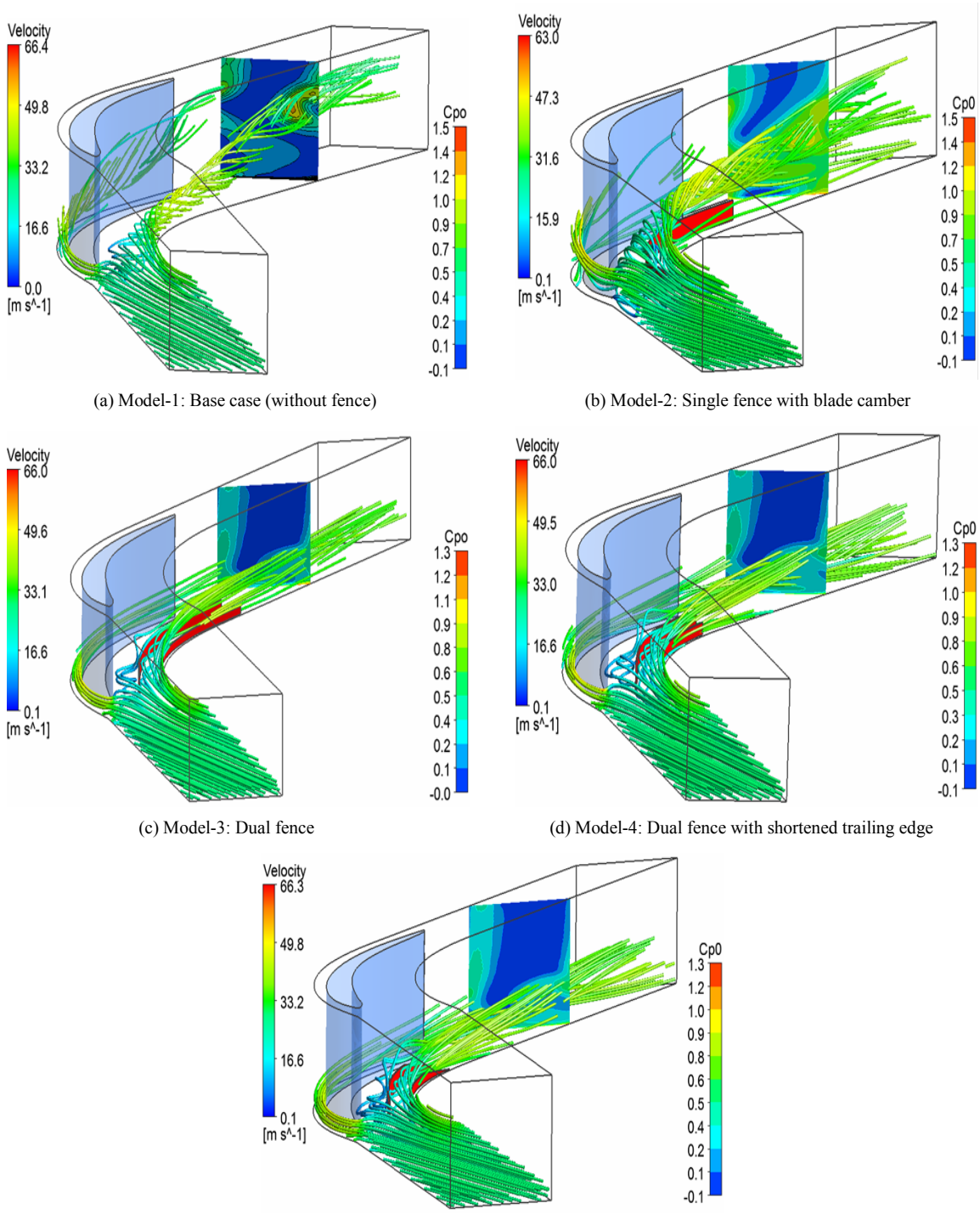

(a) Model-1: Base case (without fence)

(b) Model-2: Single fence with blade camber

(c) Model-3: Dual fence

(d) Model-4: Dual fence with shortened trailing edge

(e) Model-5: Dual fence with tapered trailing edge

Fig. 8. Contour of total pressure loss coefficient at 128 % C_{ax} superimposed with streamlines for different fence geometries.

which are difficult to capture with *RANS* [28, 29]. All these factors lead to an over prediction of the total pressure loss coefficient in *RANS* simulations. However, *RANS* simulations predicts the mean flow behavior with reasonable accuracy and it is very useful in predicting the overall performance analysis of the turbine blade.

4. Results and discussions

The result section has mainly two parts. The first part deals with the performance comparison of the five models mentioned in section-2 and explains how the dual fence model outperform the single fence model. In the second part, the

focus is given to identify a proper fence height ratio for the dual fence model. The section concludes with a detailed discussion on the aerodynamics of the optimum dual fence model.

4.1 Effect of number of fence and its geometry on loss coefficient

Detailed flow field analysis of six models have been carried out and the three dimensional flow structure, particularly near the endwall, has been shown in Fig. 8 by means of streamlines. Along with this, contours of total pressure loss coefficient also has been plotted at a distance of 50 mm downstream of the blade (i.e. 128 %C_ax). In the absence of fence (i.e. for the base case), the movement of fluid towards the suction side of the adjacent blade has been spotted. This observation is in line with the findings made by many previous researchers and this particular movement is due to the strong cross passage pressure gradient inside the boundary layer [1]. The horseshoe vortex generated near the leading edge of blade rolls up in the blade passage to form a passage vortex (Fig. 8(a)). Due to the radial pressure gradient the passage vortex migrates radially upwards along the downstream. This swirling passage is a major loss core region inside the turbine passage. At an axial location of 128 %C_ax the loss region is spotted at a spanwise location of 30 % span (S = 120 mm) from the endwall.

The above mentioned rolling up and subsequent upward movement of the flow has been weakened by keeping a single fence at half pitch (Fig. 8(b)). This modification brings down the intensity of peak loss core region but it generates significant amount of disturbances at the lower span regions. As a result, the mass averaged total pressure loss coefficient increases by 96 % (calculated at 128 % C_{ax}) compared to the base case. The fence generates the additional vortices near the leading edge of the blade which gives an adverse effect in the flow structure. These vortex generations can be prevented by modifying the leading edge of the fence, as shown for fence-1 of model-3. Further reduction in the loss coefficient is anticipated with the introduction of a double fence in the blade passage. The second fence (fence-2) helps in avoiding the cross flow towards the suction side of the adjacent blade. Mass averaged total pressure loss coefficient has decreased by 23 % in comparison with base case, even though fence-2 helps in guiding the flow along the mean-flow direction (Fig. 8(c)). In order to gain more reduction in the losses two modifications are done at the trailing edge of the fence. First one is limiting the fence length to 83 % of the axial chord (Fig. 8(d)) and the second modification is to make the trailing edge tapered. These modifications greatly reduces the rolling up and upward movement of the passage vortex (Fig. 8(e)) and resulted in 30 % reduction in the losses. The mass averaged total pressure loss coefficient for different fence geometries calculated at 128 % C_{ax} and are compared with the base case (Table 2). These values suggest that tapering of the fence at the trailing edge, contributes 6 % reduction in the overall losses. In model-4 the fences generate its own wake at the downstream. The strength of this wake diminishes by providing a tapering at the trailing end.

Table 2. Mass averaged total pressure loss coefficient for different models in comparison with base case.

Sl no.	Model	Percentage reduction in the loss coefficient in comparison with base case
1	Model-1 (base case)	-
2	Model-2	-96.22 %
3	Model-3	+23.81 %
4	Model-4	+24.33 %
5	Model-5	+29.44 %

Table 3. Details of double fence height with tapered trailing edge.

Sl No.	Fence-1 height (mm)	Fence-1 (height w.r.t span in %)	Fence-2 height (mm)	Fence-2 (height w.r.t span in %)	FHR
1	30	7.5	20	5	1.5
2	25	6.25	15	3.75	1.7
3	30	7.5	15	3.75	2
4	35	8.75	15	3.75	2.3
5	40	10	15	3.75	2.7

4.2 Effect of fence height ratio

Having understood the importance of dual fence and the trailing edge modification from the previous analysis, efforts have been put to understand the influence of the fence height on the loss coefficient. Height of both fences with respect to overall blade height in percentage is tabulated in Table 3. To this objective a parameter is defined based on the ratio of height of fence-1 to that of fence-2. This ratio is termed as fence height ratio (FHR). Simulations have been carried out for five different fence height ratios and the geometrical details are shown in Table 3. Initially the fence-1 height alone is varied keeping the fence-2 height as 15 mm. Fence-1 height is varied from 25 to 40 mm in steps of 5 mm. These models are then compared to identify an optimum fence-1 height. There must be a minimum fence height (fence-1) to break the horse shoe vortex. Beyond which increasing the fence-1 height, leads to further disturbances in the flow field. Next, the height of second fence is varied, keeping the fence-1 height constant, to get an optimum height for fence-2.

4.2.1 Effect of fence height ratio on loss coefficient

The total pressure loss coefficient is pitch mass averaged along the spanwise direction at 128 % C_{ax} for all the *FHR* cases. The span-wise variation of $\overline{C_{po}}$ for five different *FHR*, in comparison with the base case, is shown in Fig. 9. For the base case, loss coefficient increases significantly from 5 % to 30 % of span due to the rolling up of the passage vortex. The introduction of dual fence prevents this gradual rise of the

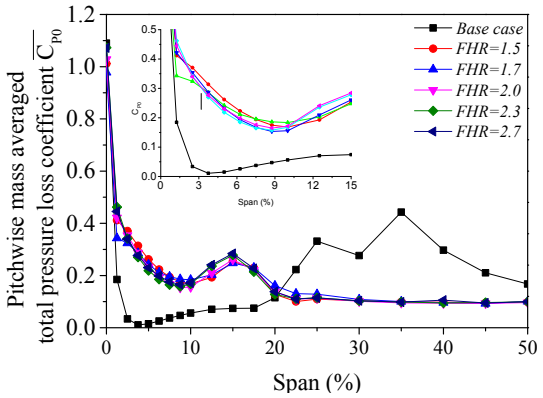

Fig. 9. Variation of pitch-wise mass averaged total pressure loss coefficient along the span.

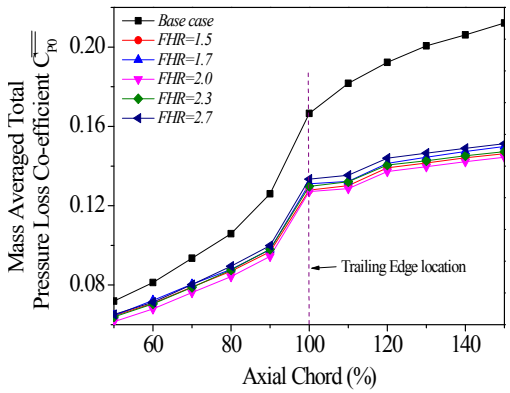

Fig. 10. Variation of area mass weighted total pressure loss coefficient along axial direction.

$\overline{C_{po}}$ value but it generates more losses near the end wall. The peak loss coefficient occurs at 15 % span for all the *FHR* cases. This shifting of peak $(\overline{C_{po}})$. towards the end wall is due to the effective breaking down of passage vortex in the blade passage. The differences in the $(\overline{C_{po}})$ with respect to *FHR* is visible only up-to 15 % of span beyond that $(\overline{C_{po}})$ varies uniformly for all the cases.

Having analysed the loss coefficient variation in the span-wise direction, the variations are noted along the axial direction also. Fig. 10 shows the area mass weighted total pressure loss coefficient $(\overline{\overline{C_{po}}})$ from 50 % axial chord (C_{ax}) to 150 % C_{ax} and it is defined as follows.

$$\overline{\overline{C_{po}}} = \frac{\int\int V_u \xi dTdS}{\int\int V_u dTdS}. \tag{3}$$

The variation of $\overline{\overline{C_{po}}}$ along the axial direction is qualitatively similar for all the dual fence models. For the base case a steep rise in $\overline{\overline{C_{po}}}$ is observed after the trailing edge, indicating high losses in the downstream side. Compared to this dual fence models exhibits rather small increase in the losses after the trailing edge. Among the tested cases *FHR* = 1.7 and 2.7 models show higher losses in the downstream side. On the other hand *FHR* = 2.0 and 2.3 exhibits least value of loss coefficient which indicate an optimum value of *FHR* lies between these two configurations. As the fence-2 height is invariant for *FHR* = 2.0 and 2.3 configurations, it naturally follows that optimum height for fence-1 lies between 30 mm and 35 mm. To understand the effect of fence-2 height on loss coefficient, fence-1 height is kept at 30 mm and fence-2 height is varied to 20 mm (*FHR* = 1.5). This configuration proves to be unworthy as the losses starts increasing in the downstream side with increase in the fence-2 height.

4.2.2 Effect of FHR on underturning and overturning

Overturning refers to larger flow deviation than expected

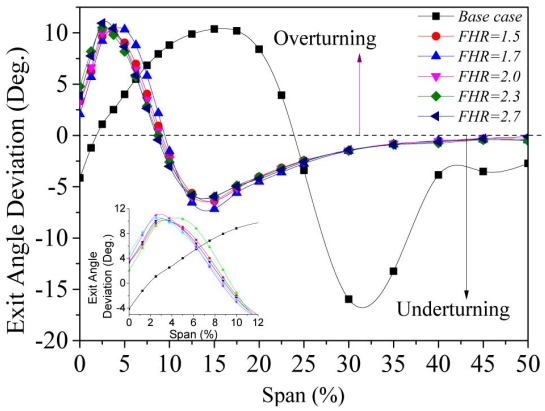

Fig. 11. Pitch-wise averaged exit flow angle deviation along the span.

from the geometrical deflection. Similarly, if flow deviation is lower than geometrical deflection of blade then it is underturning. Fig. 11 shows the exit flow angle deviations for different *FHR* configurations along the span-wise direction at an axial location of 128 % C_{ax}. It is observed that there is overturning up to 8.75 % span (*S*) for dual fence cases, beyond which the deviation changes into underturning. Maximum underturning is observed at 13.75 % of blade span for dual fence cases with a deviation of 6 deg. Severe overturning is observed for all dual fence cases at 25 % of blade span (*S* = 100 mm). In fact, the differences in deviation among the tested *FHR* cases are vivid only at 2.5 % blade span. Maximum overturning is for *FHR* = 2.7 and the least is observed for *FHR* = 1.7 and 2. Away from the end wall, from 25 % of span (*S* = 100 mm) onwards, fluid follows the exit angle of blade profile. In comparison with base case, *FHR* configurations have lower flow deviation along the span, except near the endwall. The base case exhibits severe overturning up to 20 % span, beyond that it changes to underturning till midspan. In the base case, the flow deviation occurs around 90 % of the midspan, but with the introduction of dual fence the underturning and overturning is restricted to only 30 % of overall span. This brings out one of the remarkable advantage of the dual fence.

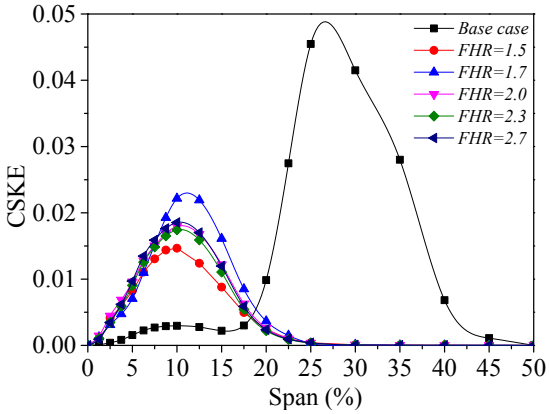

Fig. 12. Span-wise variation of pitch-wise mass averaged coefficient of secondary kinetic energy (*CSKE*) at 128 % C_{ax} .

4.2.3 Effect of fence height ratio on coefficient of secondary kinetic energy (CSKE)

The magnitude of secondary kinetic energy (*SKE*) at any plane depends on vortices caused due to viscous effect and potential flow. For inviscid flow *SKE* is proportional to the square of length of the vortex. When the mean flow increases, the *SKE* of a streamwise vortex increases [3]. The coefficient of secondary kinetic energy (*CSKE*) is defined as follows.

$$CSKE = \frac{SKE}{0.5\rho V^2} \tag{4}$$

$$SKE = 0.5\rho\left(V_{\text{sec}}{}^2 + V_w^2\right) \tag{5}$$

$$V_{\text{sec}} = -V_u \sin\alpha_2 + V_v \cos\alpha_2 . \tag{6}$$

It is observed from Fig. 12 that maximum *CSKE* is at 25 % of span from the end wall for base case. For all the *FHR* configurations, the *CSKE* has come down significantly along the entire span and the peak value occurs close to endwall. As observed in the previous section here also *FHR* = 2 emerges as the optimum configuration in terms of the minimum *CSKE* value. Beyond *S* = 30 % span the *CSKE* is almost zero for all the *FHR* configurations. With the introduction of dual fence with *FHR* = 2 the averaged CSKE has come down by 75 %.

4.3 Detailed flow field analysis of dual fence model

A detailed flow field analysis is carried out to understand the physical mechanism of dual fence in improving the flow structure within the blade passage. Fig. 13 shows the streamlines superimposed on axial vorticity contour in the base case and dual fence model (*FHR* = 2). Inside the blade passage two prominent loss core regions can be observed for the base case. The migration of the pressure side leg of horseshoe vortex within the passage is marked in Fig. 13(a) for the base case. This migration is responsible for the first loss core region within the blade passage. The suction side leg of the horse shoe vortex climbs up the blade surface and drag the low momentum boundary layer flow to the mean stream. This forms

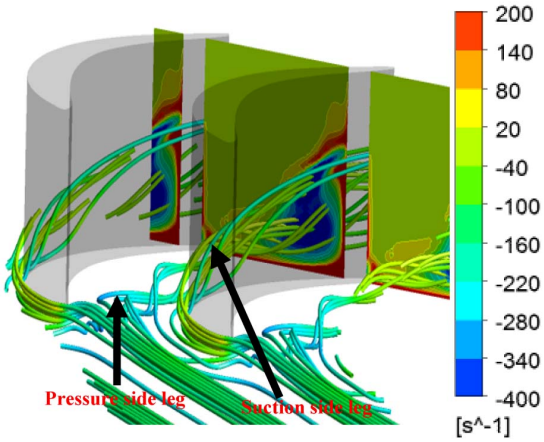

(a)

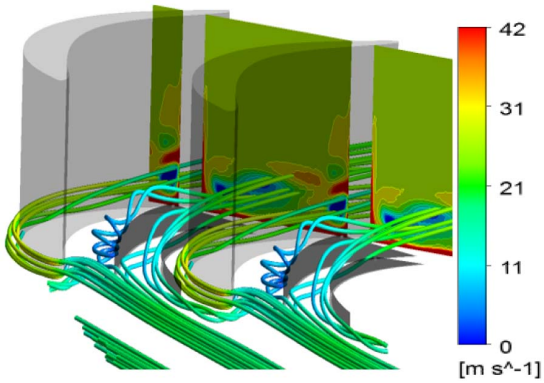

(b)

Fig. 13. Streamlines superimposed on the axial vorticity contour (a) in the base case; (b) dual fence model; *FHR = 2*.

the second loss core region. Near the trailing edge of the blade, the suction side leg and the pressure side leg meet, which results in the merging of these two loss core regions. The vorticity contours along the axial direction is shown in Fig. 13(a). It can be noted that these two loss core regions have opposite sense of rotation.

In the case of dual fence model, fence-1 breaks the pressure side leg of the horse shoe vortex at the beginning of their formation itself (Fig. 13(b)). This leads to flow disturbance and loss generation at the leading edge of the fence. However, considering the overall reduction of loss coefficient with the dual fence, this loss generation is insignificant. The role of fence-2 is to guide the flow near the suction surface of the blade thereby helping to prevent the upward movement of the suction side leg of the horse shoe vortex. The amalgamation of suction side leg of horseshoe vortex and passage vortex is avoided, preventing the accumulation of low energy fluid near the suction side of blade. The radial penetration of vortex is reduced by dual fence allowing the flow to be more stable in the midstream flow. The intensity of axial vorticity contour for dual fence case is much lower compared to the base case (Fig. 13(b)). The tapering of the fence helps to minimize the trailing edge vortex formations from these fences.

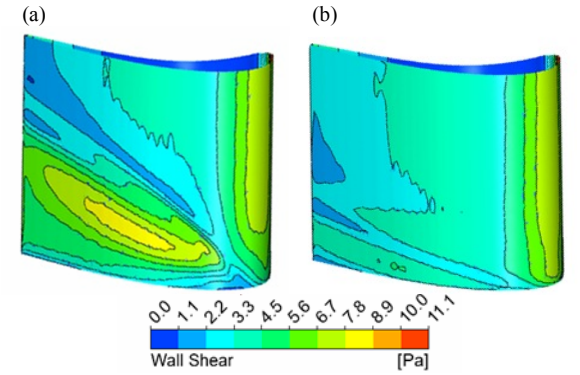

Fig. 14. Wall shear stress on the blade suction surface for (a) base case; (b) *FHR* = 2.

The wall shear stress on the blade suction surface for base case and the *FHR* = 2 configuration is shown in Fig. 14. In the base case model, a low wall shear stress region is formed over the suction surface, starting near the hub-suction surface corner and moving towards the midspan. This low wall shear stress zone can be identified as a possible region of flow separation from the blade which is basically formed due to the dragging of the low momentum fluid from the blade surface to the growing passage vortex. For the dual fence case the blade suction surface is having a uniform wall shear stress distribution in the span-wise direction.

5. Conclusions

In this computational work a dual fence with tapered trailing edge has been introduced to reduce the secondary flow losses and flow deviation in a linear turbine cascade. Computational investigations have been carried out with various configurations of streamwise fence to arrive at a suitable configuration which reduces the total pressure losses significantly in the cascade. Incorporation dual fence is successful in breaking down the vortex and weakening the end wall cross flow. Thus the amalgamation of suction side leg of horseshoe vortex and passage vortex is avoided. The accumulation of low energy fluid near the suction side of blade is minimized with this novel dual fence design. The primary fence breaks the pressure side leg of the horse shoe vortex at the beginning of their formation itself. The radial penetration of the suction side leg of the horse shoe vortex is restrained by the second fence, which helps the flow to be more stable in the midstream flow. As a result, the loss coefficient reduces significantly in the blade passage. Another remarkable achievement of dual fence is minimizing the exit flow deviation along the span. The underturning of flow is reduced in comparison with base case and results in fast recovery of exit angle deviation along the midspan.

Nomenclature

C_{ax} : Axial chord
C_{po} : Total pressure loss coefficient
C_p : Static pressure coefficient
H_p : Pressure side leg horseshoe vortex
P : Static pressure
P_0 : Total pressure
Re : Reynolds number
S : Blade span direction
S_p : Suction side leg of horse shoe vortex
T : Transverse direction
V : Velocity
V_u : Axial velocity
V_v : Tangential velocity
V_w : Radial velocity

Greek symbols

α : Exit flow angle
ρ : Density
ξ : Zeta

Abbreviations

CSKE : Coefficient of secondary kinetic energy
FHR : Fence height ratio
SKE : Secondary kinetic energy
SST : Shear stress transport

References

[1] J. Hartland, D. Gregory-Smith, N. Harvey and M. Rose, Nonaxisymmetric turbine end wall design: Part II—Experimental validation, *Jl. of Turbo*., 122 (2) (2000) 286.
[2] K. Kumar and M. Govardhan, Secondary flow loss reduction in a turbine cascade with a linearly varied height streamwise endwall fence, *International Journal of Rotating Machinery*, 2011 (2011) 1-16.
[3] J. Denton, The 1993 IGTI scholar lecture: Loss mechanisms in turbomachines, *Jl. of Turbo*., 115 (4) (1993) 621.
[4] C. Sieverding, Recent progress in the understanding of basic aspects of secondary flows in turbine blade passages, *J. Eng. Gas Turbines Power*, 107 (2) (1985) 248.
[5] J. Denton and G. Pullan, A numerical investigation into the sources of endwall loss in axial flow turbines, *ASME Turbo Expo 2012: Turbine Technical Conference and Exposition*, Copenhagen, Denmark, June 11-15 (2012) Paper No. GT2012-69173, 1417-1430.
[6] J. Horlock, Secondary flow in repeating stages of axial turbomachines, *Proc IMechE Part A: J Power and Energy,* 209 (2) (1995) 101-110.
[7] L. Langston, Secondary flows in axial turbines-A review, *Annals of the New York Academy of Sciences*, 934 (1) (2006) 11-26.
[8] R. Meyer, S. Schulz, K. Liesner, H. Passrucker and R. Wunderer, A parameter study on the influence of fillets on the compressor cascade performance, *Journal of Theoretical*

and Applied Mechanics, 50 (1) 131-145.

[9] H. Sauer, R. Müller and K. Vogeler, Reduction of secondary flow losses in turbine cascades by leading edge modifications at the endwall, *Jl. of Turbo*., 123 (2) (2001) 207.

[10] S. Mank, L. Duerrwaechter, M. Hilfer, R. Williams, S. Hogg and G. Ingram, Secondary flows and fillet radii in a linear turbine cascade, *ASME Turbo Expo 2014: Turbine Technical Conference and Exposition*, Düsseldorf, Germany, June 16-20 (2014) Paper No. GT2014-25458, V02CT38A011.

[11] G. Zess and K. Thole, Computational design and experimental evaluation of using a leading edge fillet on a gas turbine vane, *Journal of Turbomachinery*, 124 (2) (2002) 167.

[12] Y. Shi, J. Li and Z. Feng, Influence of rotor blade fillets on aerodynamic performance of turbine stage, *ASME Turbo Expo 2010: Power for Land, Sea, and Air*, Glasgow, UK, June 14-18 (2010) Paper No. GT2010-23721, 1657-166813.

[13] M. Hoeger, U. Schmidt-Eisenlohr, S. Gomez, H. Sauer and R. Müller, Numerical simulation of the influence of a fillet and a bulb on the secondary flow in a compressor cascade, *Task Quarterly*, 69 (1) 25-37.

[14] M. Govardhan, A. Rajender and J. P. Umang, Effect of streamwise fences on secondary flows and losses in a two-dimensional turbine rotor cascade, *Journal of Thermal Science*, 15 (4) (2006) 296-305.

[15] T. Kawai, Effect of combined boundary layer fences on turbine secondary flow and losses, *JSME International Journal Series B*, 37 (2) (1994) 377-384.

[16] Y. Moon and S. Koh, Counter-rotating streamwise vortex formation in the turbine cascade with endwall fence, *Computers & Fluids*, 30 (4) (2001) 473-490.

[17] T. Kawai, S. Shinoki and T. Adachi, Secondary flow control and loss reduction in a turbine cascade using endwall fences, *JSME International Journal Ser 2, Fluids Engineering, Heat Transfer, Power, Combustion, Thermophysical Properties*, 32 (3) (1989) 375-387.

[18] M. Govardhan and P. K. Maharia, Improvement of turbine performance by streamwise boundary layer fences, *Journal of Applied Fluid Mechanics*, 5 (3) (2012) 113-118.

[19] T. Poehler, J. Niewoehner, P. Jeschke and Y. Guendogdu, Investigation of nonaxisymmetric endwall contouring and three-dimensional airfoil design in a 1.5-stage axial turbine—Part I: Design and novel numerical analysis method, *Jl. of Turbo*., 137 (8) (2015) 081009.

[20] G. Brennan, N. Harvey and M. Rose, N. Fomison and M. Taylor, Improving the efficiency of the trent 500-HP turbine using nonaxisymmetric end walls—Part I: Turbine design, *Jl. of Turbo*., 125 (3) (2003) 497.

[21] G. Ingram, D. Gregory-Smith and N. Harvey, Investigation of a novel secondary flow feature in a turbine cascade with end wall profiling, *Jl. of Turbo*., 127 (1) (2005) 209.

[22] G. Ingram, D. Gregory-Smith and N. Harvey, The benefits of turbine endwall profiling in a cascade, *Proc IMechE Part A: J Power and Energy*, 219 (1) (2005) 49-59.

[23] R. J. Gustafson, Flow and temperature measurements in a linear turbine blade passage with leading edge and endwall contouring with and without film cooling, *Ph.D. Thesis*, Louisiana State University (2012).

[24] T. E. Biesinger, Secondary flow reduction techniques in linear turbine cascades, *Ph.D. Thesis*, Durham University (1993).

[25] N. Chen, Y. Xu and W. Huang, Straight-leaned blade aerodynamics of a turbine nozzle blade row with low span-diameter ratio, *Journal of Thermal Science*, 9 (1) (2000) 51-62.

[26] D. Dunn, G. C. Snedden and T. W. Von Backström, Turbulence model comparisons for a low pressure 1.5 stage test turbine, *ISABE*, Montreal, 7-11 September (2009).

[27] R. Mittal, S. Venkatasubramanian and F. M. Najjar, Large-eddy simulation of flow through a low-pressure turbine cascade, *15th AIAA Computational Fluid Dynamics Conference*, Anaheim, CA, U.S.A. 11-14 June (2001).

[28] J. Cui and P. Tucker, Numerical study of purge and secondary flows in a low-pressure turbine, *Jl. of Turbo*., 139 (2) (2016) 021007.

[29] J. Cui, R. V. Nagabhushana and P. Tucker, Numerical investigation of secondary flows in a high-lift low pressure turbine, *International Journal of Heat and Fluid Flow*, 63 (2017) 149-157.

Kiran K. N. completed M-Tech. (Research) in Thermal Engineering from NITK. Currently he is working as Design Engineer at Marmon Foods and Beverages Technologies India Pvt., Ltd., Bangalore.

S. Anish received Ph.D. from the Indian Institute of Technology Madras (IIT Madras). He is currently an Assistant Professor at the National Institute of Technology Karnataka, India. His research interests are fluid dynamics, thermodynamics, and turbomachinery aerodynamics.